Chemical Engineering Journal Advances 14 (2023) 100488

Contents lists available at ScienceDirect

Chemical Engineering Journal Advances

journal homepage: www.sciencedirect.com/journal/chemical-engineering-journal-advances

A new class of fillers in mixed matrix membranes: Use of synthetic silico-metallic mineral particles (SSMMP) as a highly selective component for CO_2/N_2 separation

Henrique Z. Ferrari [a], Daniela M. Rodrigues [a], Franciele L. Bernard [b], Leonardo M. dos Santos [b], Christophe Le Roux [c], Pierre Micoud [c], François Martin [c], Sandra Einloft [a,b,*]

[a] Post-Graduation Program in Materials Engineering and Technology, School of Technology Pontifical Catholic University of Rio Grande do Sul – PUCRS, Brazil
[b] School of Technology, Pontifical Catholic University of Rio Grande do Sul - PUCRS, Porto Alegre Brazil
[c] GET/OMP (CNRS, UT3PS, IRD, CNES), Université de Toulouse, ERT Géomatériaux, (Toulouse) France

ARTICLE INFO

Keywords:
Mixed matrix membranes
SSMMPs
CO_2/N_2 separation
Ionic liquids

ABSTRACT

Membrane-based CO_2 separation technology is a promising technology with low operating and energy costs and high scalability. This work describes the influence of synthetic silico-metallic mineral particles (SSMMP) and SSMMP/ionic liquids (IL) associated with polysulfone (PSF) to produce new mixed matrix membranes (MMM) for post-combustion technology. SSMMP is the precursor of synthetic talc undergoing no hydrothermal process resulting in a low-cost, energy-demanding, and CO_2-free emission material due to its synthesis process. SSMMP have many reactive OH groups free on their surface making this material ideal to be compatibilized in a polymeric matrix. IL was immobilized in SSMMP to further improve CO_2 affinity. As far as we know, this is the first time this material has been used to obtain MMMs. MMMs were prepared with concentrations of 0.5, 1, 2 and 3 wt % of fillers via melting solution and solvent evaporation. The obtained MMMs were characterized by scanning electron microscopy (SEM), energy dispersive spectroscopy (EDS) with elemental mapping, thermogravimetric analysis (TGA), differential scanning calorimetry (DSC) and X-ray diffraction (XRD). Permeability analyses were carried out at 25 °C and 0.4 MPa. The addition of pristine SSMMP and SSMMP/Im(nBu)Tf_2N improved membrane selectivity decreasing the permeability for the majority of tested filler content. When using SSMMP/Im(nBu)I to obtain MMMs a different behavior was observed decreasing selectivity (except for MMM with 2% (w/w) of filler) and increasing permeability in all studied concentrations. The best result was obtained for sample SSMMP/Im(nBu)Tf_2N (2% w/w) achieving a selectivity of 71.9, four times higher than pristine polysulfone membrane.

1. Introduction

The mitigation of environmental impacts caused by carbon dioxide (CO_2) emissions is urgent. The burning of fossil fuels plays an important role in climate change being imperative to capture and store the CO_2 to avoid the environmental impact this gas is causing in the atmosphere. Post-combustion CO_2 capture technology is a strong ally for this purpose separating mainly CO_2 from N_2. This technology can be adapted to most existing coal-fired power plants, absorption, adsorption, and membranes being the most important CO_2 capture technologies in this system [1–4].

The use of membranes for gas separation is increasing in industry. Membrane technology offers significant advantages, such as low capital investment and minimum energy requirements compared to the benchmark amine technology. Membrane materials can be broadly classified into polymeric, inorganic and mixed matrix membranes [5,6]. However, some challenges need to be overcome for this technology to be fully accepted in the industry, the trade-off phenomenon presented by Robeson is the most notable [7]. The ideal membrane should present high selectivity and permeability maximizing the separation. However, as permeability increases, selectivity decreases and vice versa [7,8]. One way of surpassing membrane limitations is by adding fillers to a polymeric matrix and obtaining new mixed matrix membranes (MMMs). MMMs combines the properties of a polymeric matrix with gas-selective inorganic fillers. Different fillers are being studied, including zeolites

* Corresponding author.
E-mail address: einloft@pucrs.br (S. Einloft).

https://doi.org/10.1016/j.ceja.2023.100488

Available online 3 April 2023

[9–12], silicas [13–16], carbon nanotubes [17–19], metal-organic frameworks (MOF) [20–23], and mesoporous materials, among others [24–28]. Kalantari [29] tested natural talc as filler in polysulfone polymer matrix for CO_2 removal from natural gas. Results indicate that increasing the talc content increases gas permeability, and slightly decreases selectivity. Furthermore, the thermal properties of the synthesized membranes were improved, due to the filler's superior thermal degradation properties [29]. The use of natural talc as filler to obtain MMMs is poorly described in literature while no references were found for the use of synthetic talc and SSMMP.

Natural talc is widely used in industry in a range of applications, both for material properties improvement and/or to reduce manufacturing costs. Synthetic talc emerged to overcome natural talc drawbacks, such as heterogeneity due to the different ores mixture and the difficulty of achieving small and homogeneous particles, since natural talc is amorphized after too strong grinding [30–33]. The addition of natural or synthetic talc and SSMMP to polymeric matrix aims to improve stiffness and heating resistance [31,34].

Literature describes the use of synthetic talc and SSMMP in polyurethane-based composites [35,36]. The use of synthetic talc as filler in water-based polyurethane nanocomposites obtained by in situ polymerization produced materials with superior thermal properties [35]. Interaction of hydroxyl groups present in the synthetic talc favors the interaction filler/polymer improving thermal stability. When Fe_3O_4 synthetic talc was used as filler in water-based polyurethane ferromagnetic composites, improved mechanical properties were obtained [36]. Synthetic talc was also described to improve thermal and mechanical properties of polypropylene and polyamide 6 [37]. The best result was obtained for composites synthetic talc-PA6 due to the interaction of filler polar groups and the polyamide 6.

SSMMP, the precursor of synthetic talc, is obtained at room temperature by the coprecipitation of sodium metasilicate and magnesium acetate, with an adequate Mg/Si ratio (3/4), undergoing no hydrothermal treatment as needed to obtain the synthetic talc [31,38]. It is precisely in this aspect that the advantage of SSMMP over synthetic talc resides, the lower energy expenditure for manufacturing the filler. The search for materials able to capture CO_2 with a low environmental footprint, low cost and large-scale production capacity is crucial to make this process feasible. The use of SSMMP as filler has the advantage of the low environmental impact of their synthesis when compared to zeolites, and MOFs, besides meeting the requirements to be used as filler to produce MMMs [39–41]. Another advantage of SSMMP is the presence of hydroxyl groups capable of creating strong compatibility with polymeric matrices by hydrogen bond formation. The amount of hydroxyl groups is higher in SSMMP than in synthetic talc, SSMMP being an amorphous material forming no lamellae, while synthetic talc is a crystalline material [31,34].

It is well known and described in literature [42,43] that adsorbent materials properties can be improved when modified with ionic liquids (ILs). ILs have a high affinity for CO_2 increasing mass transfer rate. ILs impregnation in porous structures of solid supports can also improve the adsorption kinetics through the formation of thin IL films on the inner walls of the solid support [44]. In mixed matrix membranes, the presence of ionic liquids usually improves permeability and/or selectivity.

Huang et al. [45] prepared Pebax mixed matrix membranes with ionic liquid-modified graphene oxide (GO). Results indicate an improvement of over 90% in CO_2/N_2 selectivity and 50% in CO_2 permeability for the GO-IL MMMs compared to the pure Pebax membrane. Furthermore, the incorporation of IL-NH_2 improved the interfacial interaction and the filler-polymer compatibility.

Polysulfone membranes are well described in literature due to their good properties, such as thermal and mechanical resistance, high tensile strength and pressure resistance. It also exhibits significant resistance to acidic or basic environments, over a significant range of concentrations and temperatures [46,47]. Numerous studies have been carried out using polysulfone as a polymeric matrix in MMMs with good results [48–52].

In the present work, SSMMP and SSMMP functionalized with IL, Im(nBu)Tf_2N or Im(nBu)I, were used as fillers in the polysulfone polymer matrix to obtain new MMMs. Obtained membranes were tested in a CO_2/N_2 mixture. Pristine polysulfone membrane selectivity and permeability for the CO_2/N_2 mixture were evaluated and used to compare with the performances of synthesized MMMs. According to literature, no previous study was found on MMMs using SSMMP as fillers indicating that these results can open new perspectives and future research.

2. Materials and methods

2.1. Materials

Polysulfone (pellets) with an average molar mass of approximately 35,000 was purchased from Sigma Aldrich. Tetrahydrofuran (99% purity) used as solvent was obtained from Dinâmica, Brazil. The CO_2 and N_2 gasses (purity of 99.80% and 99.99%, respectively), were purchased from White Martins. For SSMMP production, sodium metasilicate pentahydrate was obtained from Dinâmica, Brazil, and magnesium acetate tetrahydrate from Merck (purity of 99.5%). For SSMMP/ionic liquids production, the reagents sodium iodide and lithium salt of bis(trifluoromethane)sulfonimide [$LiTf_2N$], were purchased from Sigma Aldrich. All chemicals were used without further purification. 1-(triethoxysilylpropyl)-3-n-butylimidazolium chloride [Im(nBu)-Cl-silane] was made in GET laboratory.

2.2. Synthesis of SSMMP

SSMMP was obtained following literature procedures at room temperature and adequate Mg/Si ratio [31,33]. The Si source is sodium metasilicate pentahydrate ($Na_2SiO_3.5(H_2O)$) and Mg source is magnesium tetrahydrate ($Mg(CH_3COO)_2.4(H_2O)$). Two solutions were prepared. In the first one, the sodium metasilicate pentahydrate was dissolved in water. In the second one, magnesium acetate tetrahydrate was solubilized in water and acetic acid. Then solution 2 was added to solution 1 under constant stirring. The obtained precipitate was washed in distilled water and centrifuged 3 times to remove sodium acetate, and dried in an oven at a temperature of 100 °C for 48 h.

2.3. Synthesis of SSMMP/IL

SSMMP/IL were synthesized using procedures described in literature (WO2013093339, [38]). They are obtained by functionalizing the SSMMP by replacing 5% of the Si source (sodium metasilicate pentahydrate) by Im(nBu)-Cl-silane. The Cl^- anion is exchanged by Tf_2N anion using $LiTf_2N$, forming Im(nBu)Tf_2N, or by I using sodium iodide to obtaining Im(nBu)I [38]. See Figure S1 for SSMMP/IL structure.

2.4. MMMs preparation

Mixed matrix membranes were prepared following the procedure of melting solution and solvent evaporation. The polymer matrix and fillers were dried at 70 °C for 24 h before starting the process. Pristine membrane was prepared by mixing 2 g of polysulfone in 20 mL of THF. The mixture was kept under constant agitation for 24 h, then poured into a Petri plate and placed for 48 h in a closed container under an inert atmosphere to delay the solvent evaporation and avoid bubbles formation and moisture. A similar protocol was used to produce the MMMs with SSMMP and SSMMP/IL (SSMMP/Im(nBu)Tf_2N and SSMMP/Im(nBu)I). Initially, fillers are stirred with an adequate amount of THF (10 ml per gram) for 2 h. Then, the polysulfone is added in the amount necessary to form the membranes with 0.5%, 1%, 2% and 3% by mass of filler. The filler/polysulfone solution was stirred for 24 h at room temperature. After this time, the mixture is sonicated for 10 min in ultrasound to

efficiently disperse the filler. Subsequently, the solution is poured into a Petri plate and follows the drying process identical to the pristine membrane. All membrane thickness values were measured using a micrometer in different regions of the sample. The thickness values were found to range from 80 to 120 μm.

The produced membranes were identified according to the filler content and type. The membranes with SSMMP received the label PSF-SSMMP 0.5wt%, PSF-SSMMP 1wt%, PSF-SSMMP 2wt%, PSF-SSMMP 3wt%. Samples with SSMMP/IL were labeled PSF-SSMMPIm(nBu)Tf_2N 0.5wt%, PSF-SSMMP/Im(nBu)Tf_2N 1wt%, PSF-SSMMP/Im(nBu)Tf_2N 2wt%, PSF-SSMMP/Im(nBu)Tf_2N 3wt% for the anion Tf_2N. Samples with SSMMP/IL with the anion I were labeled PSF-SSMMP/Im(nBu)I 0.5wt%, PSF-SSMMP/Im(nBu)I 1wt%, PSF-SSMMP/Im(nBu)I 2wt%, PSF-SSMMP/Im(nBu)I 3wt%. The pristine membrane was labeled PSF.

2.5. Characterization

2.5.1. BET

SSMMP surface area was calculated using the method developed by Brunauer-Emmett-Teller (BET). The N_2 adsorption and desorption isotherms were determined at 77 K, using the Quantachrome NOVA 4200e equipment. The samples were previously treated for 20 h at 120 °C under vacuum.

2.5.2. NMR

SSMMP solid-state nuclear magnetic resonance (NMR) experiments were recorded on a Bruker Avance 400 spectrometer equipped with a 4 mm probe operating at 399.60 MHz for ^{1}H and 79.39 MHz for ^{29}Si. Samples were rotated at the magic angle at a frequency of 5 kHz in 4 mm diameter rotors at room temperature. The ^{29}Si MAS-NMR spectra were obtained by a single pulse sequence with a recycle delay of 10.0 s.

2.5.3. SEM/EDS/Mapping

SSMMP morphology, as well as the evaluation of filler distribution in the polysulfone polymeric matrix, were carried out by scanning electron microscopy (SEM) technique. Philips Model XL 30 Microscope, equipped with EDS and Mapping was used. The EDS and Mapping analyzes were used to confirm the membrane distribution of the constituent elements.

2.5.4. AFM

AFM analysis was performed in the peak force tapping mode using a Bruker Dimension Icon PT equipped with TAP150A probe (Bruker, resonance frequency of 150 kHz and 5 Nm^{-1} spring constant). The scanned area of the images was 5 μm × 5 μm with a resolution of 512 frames per area.

2.5.5. TGA

TGA analysis was used to verify the influence of SSMMP on the thermal stability of PSF membranes. MMMs were tested from 25°C to 800°C, with a heating rate of 10°C/min under N_2 atmosphere.

2.5.6. DSC

Differential scanning calorimetry was performed to determine the glass transition temperature (Tg) of the MMMs. TA Instrument Q20 differential scanning calorimeter in the range 0 °C – 250 °C and heating rate of 10 °C/min under nitrogen atmosphere was used for analysis.

2.5.7. FTIR

FTIR analysis was used to verify the typical bonds of SSMMP and SSMMP/IL. PerkinElmer Frontier FT-IR spectrometer with wavelengths from 600 cm^{-1} to 4000 cm^{-1} was used.

2.5.8. XRD

MMMs and SSMMP were analyzed by XRD (X-ray Diffraction) to evaluate the crystallinity when inserting the inorganic filler into the polymer matrix. The test was performed on a D8 Advance A25 X-ray Diffractometer (Bruker).

Table 1
Textural properties of SSMMP.

Sample	S_{BET} ($m^2\ g^{-1}$)
SSMMP	300.4
SSMMP/Im(nBu)Tf_2N	151.0
SSMMP/Im(nBu)I	156.0

2.6. Permeability tests

CO_2 and N_2 permeability and selectivity of the membranes were evaluated using a system consisting of two plates and tests carried out in triplicate. A cavity of 4 cm in diameter is present between the two plates where the membrane was inserted. Initially, vacuum is performed on the membrane and system before feeding the gasses. CO_2 or N_2 are fed at a pressure of 4 bar. At the bottom, a pressure transducer computes the amount of gas passing through the membrane over time (dP/dt). Permeability was determined from the slope (dP/dt) of the linear portion of the pressure versus time curve using Eq. (1) [53,54].

$$Permeability = \frac{273.15\ l\ V}{76\ PAT}\left(\frac{dP}{dt}\right) \quad (1)$$

Where Permeability is the permeation coefficient in cm^3(STP)cm/(cm^2.s.cmHg) [1Barrer = 1×10^{-10} cm^3(STP)cm/(cm^2.s.cmHg)], l is the membrane thickness (cm), P is the feed pressure; A corresponds to the membrane area (cm^2); V is the permeation cell volume (cm^3); T is the experimental temperature (K).

The ideal selectivity was calculated from Eq. (2), dividing CO_2 and N_2 permeabilities.

$$\alpha_{CO_2N_2} = \frac{P_{CO2}}{P_{N2}} \quad (2)$$

The solution-diffusion mechanism is widely accepted as the primary transport mechanism for gas permeation through a dense membrane [55]. In this mechanism, the gas solubility coefficient (cm^3(STP)/(cm^3 cmHg)) is calculated using Eq. (3).

$$S = \frac{P}{D} \quad (3)$$

Where P represents the permeability and D the gas diffusion coefficient (cm^2/s).

The gas diffusion coefficient was determined using the time-lag method, which is described by Eq. (4) [56].

$$D = \frac{l^2}{6\theta} \quad (4)$$

Where D is diffusion coefficient (cm^2/s), l is the membrane thickness (cm) and θ is the diffusion time lag (s)determined by the linear portion of the curve when intercepting the time-axis.

3. Results and discussion

3.1. Characterization of SSMMP and SSMMP/IL

Aiming to investigate the synthesized SSMMP and SSMMP/IL properties, a series of characterizations were performed. Table 1 presents the textural properties of pristine SSMMP and SSMMP/ILs.

Specific surface area of SSMMP is 300.4 m^2/g, higher when compared to natural and synthetic talc, 20 m^2/g and 125 m^2/g, respectively [38]. For samples SSMMP/IL, a reduction in specific surface area was evidenced [57]. Similar results were reported in the literature, as described by Shi and coworkers [58] for supported ionic liquids in SBA-15 and for Mohamedali and coworkers [44] when immobilizing [bmim][Ac] on MCM-41 and SBA-15. Solids with higher specific surface

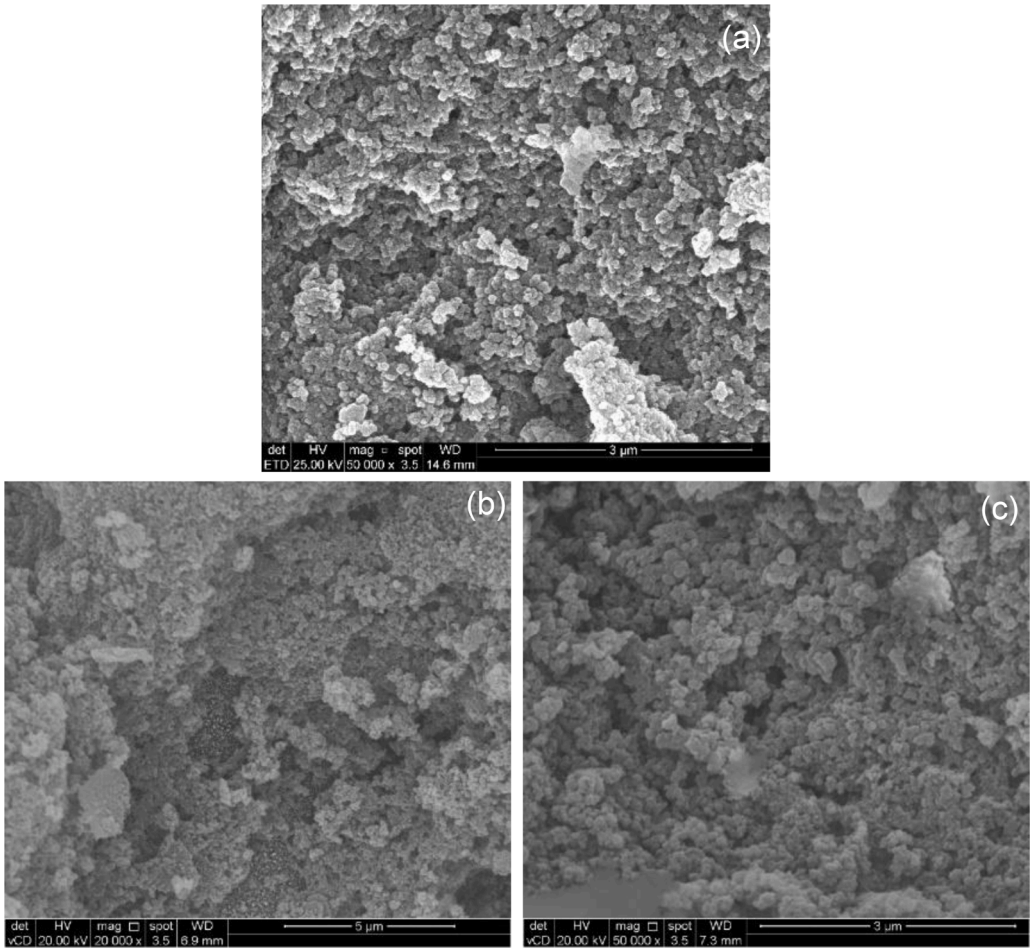

Fig. 1. SEM image of fillers: (a) SSMMP, (b) SSMMP/Im(nBu)I and (c) SSMMP/Im(nBu)Tf_2N.

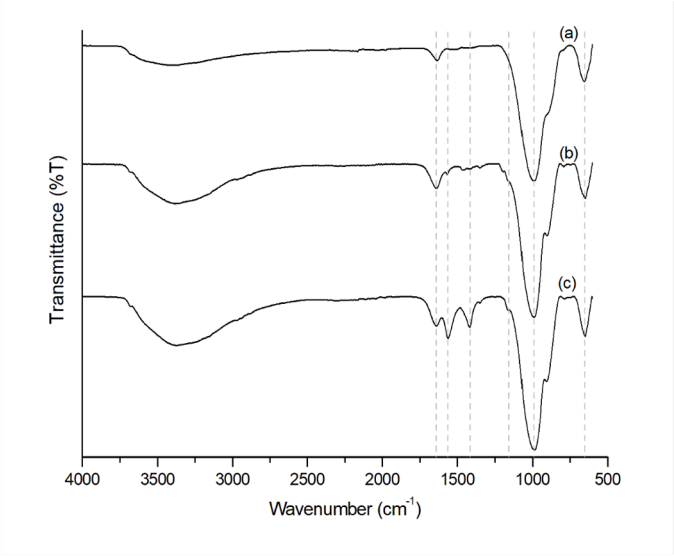

Fig. 2. FTIR spectra of (a) SSMMP, (b) SSMMP/Im(nBu)Tf_2N and (c) SSMMP/Im(nBu)I.

area present a greater number of available active sites resulting in greater adsorption capacity [59]. Besides, the production of the SSMMP is substantially simpler, with less energy expenditure than the production of synthetic talc, corroborating why SSMMP was chosen as a filler for MMMs.

Fig. 1 shows SEM images for pristine SSMMP and SSMMP/IL. SSMMP consists of an agglomerate of granules-type particles with relatively regular particle sizes. For SSMMP/Im(nBu)Tf_2N and SSMMP/Im(nBu)I, images like pristine SSMMP were obtained evidencing that the ILs have no visible influence on filler morphology.

Fig. 2 shows FTIR spectra for pristine SSMMP and SSMMP/ILs. A wide band vibration between 3400 and 3500 cm^{-1} is associated with the OH stretching vibrations of water molecules, while at 1635 cm^{-1} is associated with their bending vibrations [60,61]. The small band around 3676 cm^{-1} is attributed to stretching vibration of OH groups involving Si and/or Mg cations. The band near 1000 cm^{-1} is attributed to Si–O stretching modes. The band at 655 cm^{-1} corresponds to OH vibration.

Fig. 2((b) and (c)) shows the spectra of SSMMP/Im(nBu)Tf_2N and SSMMP/Im(nBu)I, respectively. Three new bands are observed at 1560 cm^{-1} attributed to C=C of imidazolium cation, at 1440 cm^{-1} to ILs CH_2 deformation and at 1140 cm^{-1} related to Si-C bond of imidazolium side chain [38].

Figure S2 presents the SSMMP and SSMMP/IL thermal degradation analysis. The pristine SSMMP presents three thermal decomposition events. The first one occurs near 110 °C, corresponding to moisture loss. The second occurs from 110 °C to 800 °C, associated with the loss of hydroxyl groups bonded to silicon and/or magnesium atoms and present at the surface of SSMMP [38]. For samples functionalized with ILs, the first loss event is attributed to moisture and the second to the degradation of imidazolium cation in addition to the loss of hydroxyl groups present at the surface of SSMMP [38]. SSMMP/Im(nBu)Tf_2N evidenced superior thermal stability than SSMMP/Im(nBu)I.

Figure S3 presents the DRX of SSMMP and SSMMP/IL. All samples

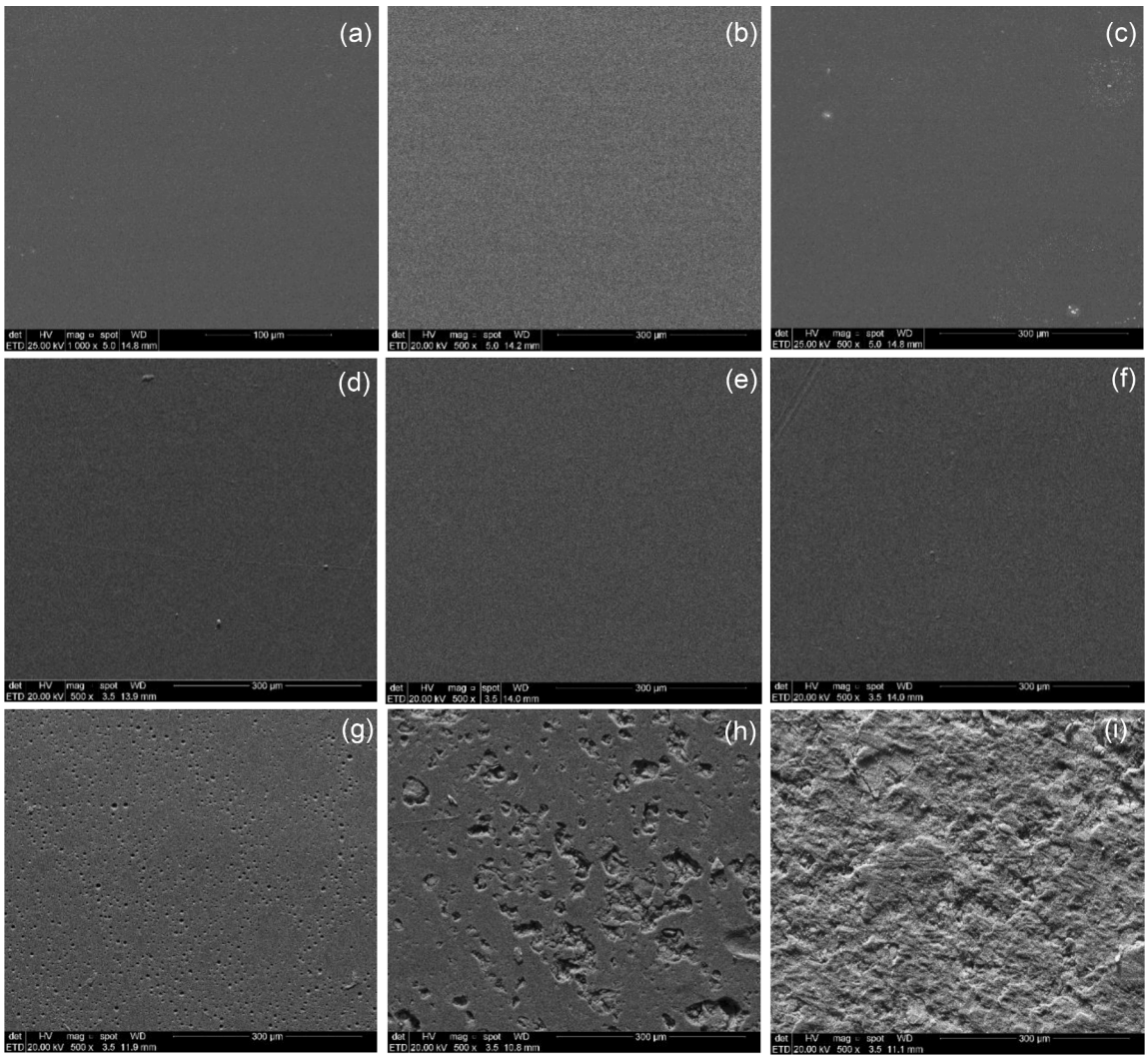

Fig. 3. . MMMs SEM images: (a) bare PSF, (b) PSF-SSMMP 0.5 wt%, (c) PSF-SSMMP 3wt%, (d) PSF-SSMMP/Im(nBu)Tf_2N 0.5wt%, (e) PSF-SSMMP/Im(nBu)Tf_2N 2wt %, (f) PSF-SSMMP/Im(nBu)Tf_2N 3wt%, (g) PSF SSMMP/Im(nBu)I 1wt%, (h) PSF-SSMMP/Im(nBu)I 2wt%, (i) PSF-SSMMP/Im(nBu)I 3wt%.

present an X-ray diffraction pattern with low-intensity and broad diffraction peaks, confirming the amorphous structure and lower stacking order and growth in the ab plane [34,38].

^{29}Si NMR spectra (Figure S4) show 2 main signals for SSMMP at −85.5 and −92.7 ppm corresponding to Q-type Si atoms (with Si-O-Si, Si-O-Mg and Si-OH bonds), Q^1 (around −85.5) and Q^2 (around −92,7) for the most part because of the small TOT entities of the SSMMP [31]. For selective CO_2 separation from gas streams, the design of materials with hydroxyl groups can enhance selectivity. Literature describes that increasing polar groups in sorbent surfaces increase the CO_2 sorption capacity and selectivity [62].

3.2. MMMs characterization

3.2.1. Morphology

MMMs SEM images are shown in Fig. 3. For membranes with bare SSMMP (Fig. 3b and c), a good dispersion was achieved for samples with low filler content. When adding 3 wt% of filler, some filler agglomerates are evidenced indicating a maximum filler content is supported to produce uniform membranes.

For MMMs using SSMMP/Im(nBu)Tf_2N (Fig. 3d, e, and f), even with higher filler concentration, uniform membranes were obtained with no agglomerates. Better morphological characteristics for MMMs using SSMMP/Im(nBu)Tf_2N as filler indicate the importance of the IL in the filler dispersion into the polymeric matrix. Unlike SSMMP/Im(nBu)Tf_2N, the use of SSMMP/Im(nBu)I (Fig. 3g, h and i) provided a poor compatibility filler/polysulfone matrix for all filler content. As seen in SEM images, filler agglomerates can be observed increasing with filler concentration.

SSMMP/Im(nBu)I sample surface magnification was performed (see Figure S5). As seen, cavities are visible on the surface and, filled by the filler, corroborating the poor compatibility of filler/polysulfone. According to research by Yang et al. [63], powdered natural talc is reported to be non-porous. By similarity, the unitary sheet of SSMMP is non-porous too. However, the small particle size of SSMMP results in a high specific surface area [33], which increases its hydrophilicity [30]. This increased hydrophilicity enhances its compatibility with hydrophilic polymers, unlike PSF, which is a hydrophobic polymer [64,65]. Therefore, adding a hydrophobic anion like Tf_2N [66] to the SSMMP structure promotes filler/polymer compatibility. On the other hand, the I anion gives the filler a hydrophilic character [67,68], which makes filler/polymer compatibility difficult.

MMMs Cross-sectional images are shown in Figure S6. Compared to bare PSF (Fig S6a), the MMMs present similar cross-sectional images for MMMs with low filler content of bare SSMMP (Fig S6b) and SSMMP/Im(nBu)Tf_2N (Fig S6c). MMMs gradually became more uneven with filler addition. For PSF-SSMMP/Im(nBu)I 0.5wt% (Fig S6d), some incompatibility filler/polymer can be seen, and for PSF-SSMMP/Im(nBu)I

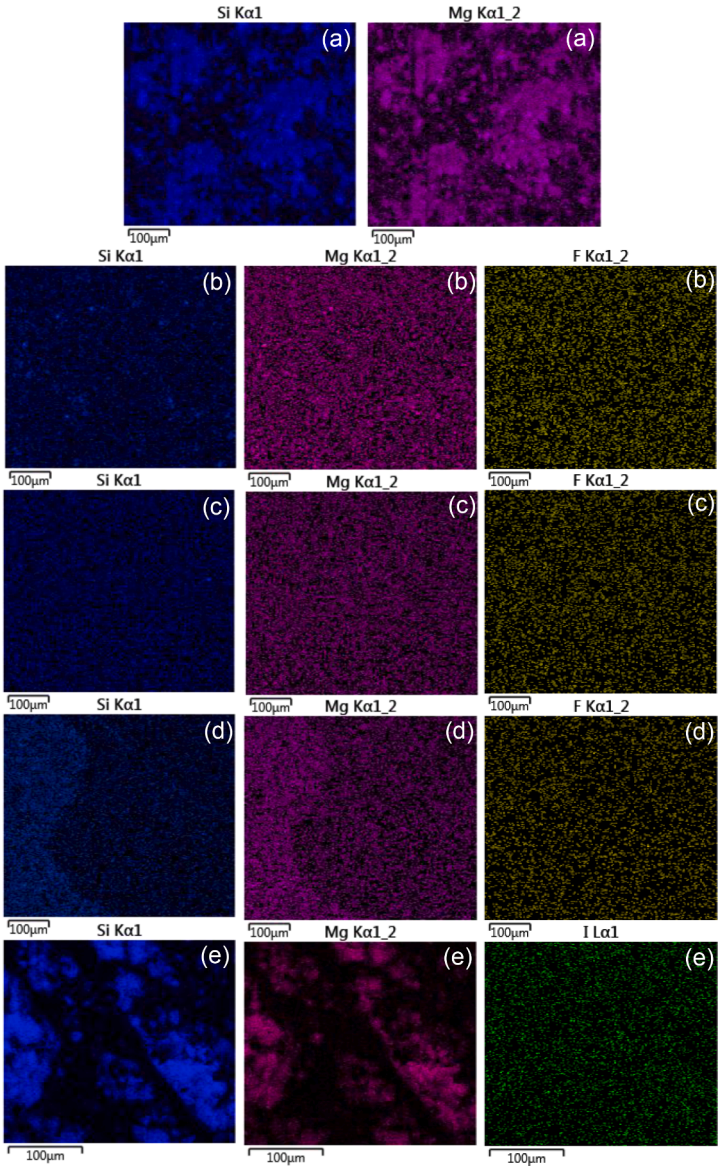

Fig. 4. Mapping of MMMs: (a) PSF-SSMMP 3wt%, (b) PSF-SSMMP/Im(nBu)Tf_2N 0.5wt%, (c) PSF-SSMMP/Im(nBu)Tf_2N 2wt%, (d) PSF-SSMMP/Im(nBu)Tf_2N 3wt%, (e) PSF-SSMMP/Im(nBu)I 2wt%.

3 wt% (Fig S6e), the incompatibility is higher to form two phases in the membrane. Importantly, the cavities in SSMMP/Im(nBu)I are present only on the surface.

3.2.2. *EDS/Mapping*

As seen in EDS analysis (see Table S1), all samples show carbon, oxygen and sulfur from PSF matrix. SSMMP-containing samples present also magnesium and silicon. When Im(nBu)Tf_2N and Im(nBu)I are incorporated into MMMs, fluorine and iodine are evidenced. For MMMs with SSMMP/Im(nBu)I, no behavior of proportionality between filler amount and element concentration is observed, probably due to low polymer/filler compatibility.

Fig. 4 shows MMMS EDS mapping results. For sample with 3wt% of SSMMP (Fig. 4a), cluster formation can be identified, like that seen in Fig. 3c. For samples PSF-SSMMP/Im(nBu)Tf_2N (Fig. 4b, c and d), a uniform filler distribution is observed regardless the filler content indicating that the Im(nBu)Tf_2N acts like a compatibilizer agent. PSF-SSMMP/Im(nBu)I (Fig. 4e) showed a different behavior evidencing that, unlike Tf_2N, I present no filler/polymer compatibilizer effect (compare Fig. 4b,c,d and e).

3.2.3. *Thermal stability*

MMMs organic and inorganic phases good compatibility is a fundamental requirement for large-scale applications contributing to a more efficient CO_2 separation, increasing selectivity, besides contributing to membrane stability and resistance [27,69]. Fig. 5 shows TGA for bare PSF membrane and MMMs. Thermogram of bare PSF membrane reveals a single weight loss occurring at a maximum temperature of 540°C in agreement with literature [70]. The weight loss is attributed to PSF backbone thermal decomposition [71]. The residual weight of bare PSF at 800 °C was 31.9% attributed to the aromatic fraction in the PSF main chain producing thermally stable carbonaceous constituents during degradation [72].

For membranes with SSMMP, SSMMP/Im(nBu)Tf_2N and SSMMP/Im (nBu)I, the thermograms indicate two weight losses, one related to the PSF degradation around 540 °C and the other at a maximum temperature of approximately 170°C. Furthermore, we can note that the MMMs filled with SSMMP are a little bit more stable than the other MMMs (bare PSF or SSMMP/IL). This may be due to a better crystallinity of the PSF matrix when filled with SSMMP which improves it, contrary to the ones filled with SSMMP/IL which are a little bit less stable than PSF. It seems

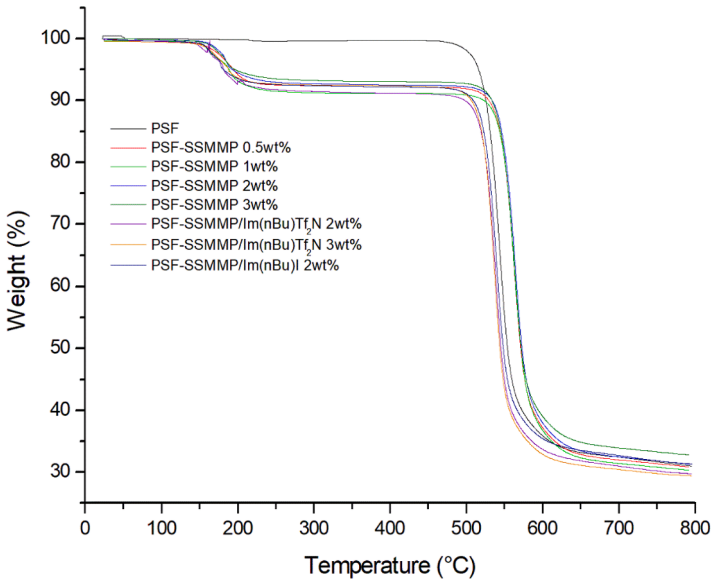

Fig. 5. TGA for MMMs samples.

Table 2
Tg for MMMs PSF-SSMMP and PSF-SSMMP/IL.

Membranes	Tg (°C)
PSF	185.17
PSF- SSMMP 0.5 wt%	185.32
PSF- SSMMP 1 wt%	185.93
PSF- SSMMP 2 wt%	185.36
PSF- SSMMP 3 wt%	186.92
PSF- SSMMP/Im(nBu)Tf_2N 0.5 wt%	186.83
PSF- SSMMP/Im(nBu)Tf_2N 1 wt%	186.18
PSF- SSMMP/Im(nBu)Tf_2N 2 wt%	180.39
PSF- SSMMP/Im(nBu)Tf_2N 3 wt%	184.59
PSF- SSMMP/Im(nBu)I 0.5 wt%	187.91
PSF- SSMMP/Im(nBu)I 1 wt%	183.90
PSF- SSMMP/Im(nBu)I 2 wt%	184.24
PSF- SSMMP/Im(nBu)I 3 wt%	185.57

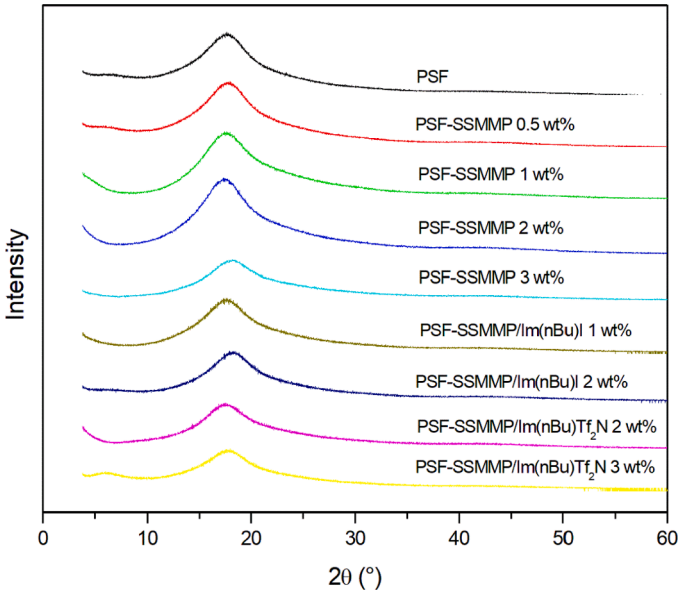

Fig. 6. XRD of obtained MMMs.

Table 3
Surface roughness parameters of bare PSF membrane and MMMs.

Membrane	Rq (nm)	Ra (nm)	Rmax (nm)
PSF	6.04	4.32	123.0
PSF-SSMMP 0.5wt%	1.98	1.32	91.9
PSF-SSMMP 3wt%	20.4	16.3	158.0
PSF-SSMMP/Im(nBu)Tf_2N 2wt%	10.5	7.90	80.0
PSF-SSMMP/Im(nBu)Tf_2N 3wt%	9.02	4.76	144.0
PSF-SSMMP/Im(nBu)I 1wt%	13.4	9.81	140.0
PSF-SSMMP/Im(nBu)I 2wt%	14.7	11.3	130.0

compatible with the possible fact that IL act as plasticizing agent in PSF matrix (see a few lines further in the article, on the Tg values).

3.2.4. DSC

Polysulfone is an amorphous polymer. Table 2 shows filler effect in Tg of the MMMs.

The Tg of bare PSF membrane was 185.17 °C, close to values reported in literature [50,73]. MMMs Tg values are very close to bare PSF membrane showing that the filler introduction has no effect on PSF chain dynamics [74].

For sample PSF-SSMMP/Im(nBu)Tf_2N 2wt%, the change in Tg value was more evident being reduced compared to bare PSF. This result is probably related to the IL acting as a plasticizing agent in this filler content providing additional conformational flexibility and improved polymer/filler compatibility [72,75]. Precisely with this sample, the best selectivity result was obtained.

3.2.5. XRD

Fig. 6 presents XRD analysis for MMMs. PSF sample presents a characteristic peak at 17° The XRD of MMMs PSF-SSMMP are similar to bare PSF (except for 3%) even SSMMP being amorphous (see Figure S3). For the sample with 3% of filler, a decrease in peak intensity is observed which can be related to the formation of the agglomerate.

For samples PSF-SSMMP/IL, a slight decrease in the peak intensity is observed. The IL/PSF matrix interaction is probably interfering in the polymer chain organization as described in literature. Estahbanati et al. [76] described Pebax membranes with ionic liquids. According to their findings, the increase in IL content decreases the hydrogen bonds increasing membrane amorphous character. The same behavior was observed for gel membranes (PVDF-HFP) and [bmim][BF_4]. The IL

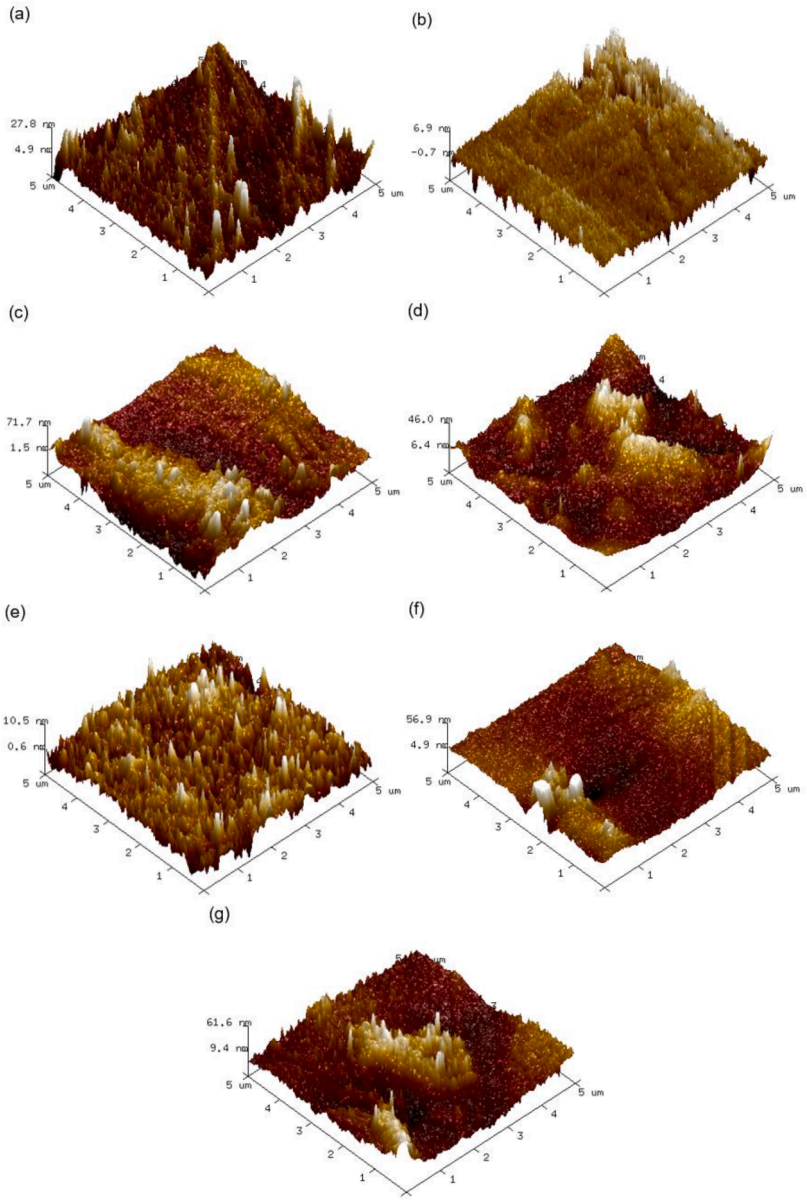

Fig. 7. AFM images of MMMs: a) bare PSF, b) PSF-SSMMP 0.5wt%, c) PSF-SSMMP 3wt%, d) PSF-SSMMP/Im(nBu)Tf_2N 2wt%, e) PSF-SSMMP/Im(nBu)Tf_2N 3wt%, f) PSF-SSMMP/Im(nBu)I 1wt%, g) PSF-SSMMP/Im(nBu)I 2wt%.

addition modified the matrix crystallinity due to the complexation of the IL cation with the polymeric matrix [77].

3.2.6. AFM

AFM analysis allows a more detailed investigation of the MMMs surface. Table 3 presents values of mean roughness (Ra), mean square roughness (Rq) and maximum height roughness (Rmax). Fig. 7 presents the three-dimensional images of the prepared membranes. The light areas stand to the highest points and the dark areas to the valleys of the membranes [78]. Filler addition promotes rearrangements in polymer matrix structure due to the Van der Waals forces adhesion of the filler particles/membrane surface [51]. The MMMs presented a higher roughness than the bare PSF membrane, except in the PSF-SSMMP 0.5wt % sample, for which the roughness was lower. The punctual light areas present in the pure polysulfone were transformed into a region exclusively dominated by the light area (see Fig. 7b) indicating the replacement of large peaks by several small peaks in the sample PSF-SSMMP 0.5wt%. Literature describes similar behavior for the incorporation of graphene oxide in polyethersulfone [79] and clay in PSF [29], with both

Table 4
Permeability and ideal selectivity for MMMs PSF-SSMMP, PSF-SSMMP/Im(nBu)Tf_2N and PSF-SSMMP/Im(nBu)I.

Membrane	P_{CO2} (barrer)[1]	P_{N2} (barrer)[1]	$\alpha_{CO2/N2}$[1]
PSF	4.73 ± 0.34	0.26 ± 0.07	18.2
PSF-SSMMP 0.5wt%	2.82 ± 0.05	0.048 ± 0.02	59.3
PSF-SSMMP 1wt%	1.96 ± 0.15	0.064 ± 0.00	30.9
PSF-SSMMP 2wt%	2.18 ± 0.01	0.048 ± 0.01	45.3
PSF-SSMMP 3wt%	1.85 ± 0.30	0.039 ± 0.00	47.9
PSF-SSMMP/Im(nBu)Tf_2N 0.5wt%	3.10 ± 0.50	0.046 ± 0.02	67.3
PSF-SSMMP/Im(nBu)Tf_2N 1wt%	3.20 ± 0.52	0.069 ± 0.01	46.7
PSF-SSMMP/Im(nBu)Tf_2N 2wt%	4.03 ± 0.30	0.056 ± 0.00	71.9
PSF-SSMMP/Im(nBu)Tf_2N 3wt%	10.60 ± 1.15	0.34 ± 0.05	31.6
PSF-SSMMP/Im(nBu)I 0.5wt%	10.57 ± 0.43	1.32 ± 0.08	8.0
PSF-SSMMP/Im(nBu)I 1wt%	16.52 ± 1.22	1.30 ± 0.08	12.7
PSF-SSMMP/Im(nBu)I 2wt%	9.62 ± 0.23	0.39 ± 0.20	24.3
PSF-SSMMP/Im(nBu)I 3wt%	6.90 ± 0.38	0.69 ± 0.05	10.1

[1] Temperature of 25 °C and CO_2 and N_2 pressure of 4 bar.

Table 5
Diffusion and solubility coefficients for pristine PSF and SSMMPs based MMMs at 4 bar and 25 °C.

Membrane	Diffusion coefficient for CO_2 (x 10^{-8} cm^2/s)	Solubility coefficient for CO_2 (10^2 cm^3(STP)/cm^3 cmHg)
PSF [a]	1.17 [a]	≈ 2.6 [a]
PSF	1.48 ± 0.05	3.15 ± 0.11
PSF-SSMMP 0.5wt%	0.96 ± 0.03	2.92 ± 0.07
PSF-SSMMP 1wt%	0.71 ± 0.07	2.75 ± 0.04
PSF-SSMMP 2wt%	0.75 ± 0.11	2.90 ± 0.10
PSF-SSMMP 3wt%	0.62 ± 0.10	2.94 ± 0.09
PSF-SSMMP/Im (nBu)Tf_2N 0.5wt%	1.36 ± 0.09	2.27 ± 0.07
PSF-SSMMP/Im (nBu)Tf_2N 1wt%	1.35 ± 0.06	2.37 ± 0.08
PSF-SSMMP/Im (nBu)Tf_2N 2wt%	1.47 ± 0.03	2.73 ± 0.05
PSF-SSMMP/Im (nBu)Tf_2N 3wt%	3.84 ± 0.05	2.75 ± 0.10
PSF-SSMMP/Im (nBu)I 0.5wt%	4.21 ± 0.13	2.50 ± 0.12
PSF-SSMMP/Im (nBu)I 1wt%	5.61 ± 0.19	2.94 ± 0.12
PSF-SSMMP/Im (nBu)I 2wt%	3.63 ± 0.16	2.65 ± 0.11
PSF-SSMMP/Im (nBu)I 3wt%	2.60 ± 0.10	2.66 ± 0.08

[a] Values obtained from the study by Kim et al. (2007), carried out at a pressure of 4 bar, using the time-lag method.

authors describing the decrease of peaks and valleys resulting in a smoother surface. For the other samples, the increase in membrane roughness is possibly linked to low dispersion and to filler accumulation corroborated by SEM images and XRD analyses (see Fig. 6) (compare PSF-SSMMP 3wt% (Fig. 3c) with high roughness and the bare PSF membrane (Fig. 3a). PSF-SSMMP/Im(nBu)I samples also presented a higher roughness compared to bare PSF (see agglomerates in Figure S5) corroborating the low compatibility filler/matrix.

3.3. CO_2/N_2 separation performance

Table 4 and Figure S7 present the ideal selectivity and pure gas permeability results for bare PSF membrane and MMMs.

It is interesting to note that in membranes with SSMMP, the permeability for CO_2 and N_2 decreases, being sharper for N_2. SSMMP addition increases selectivity, achieving maximum value of 59.3 when 0.5 wt% of SSMMP is added. For all MMMs, a higher CO_2 selectivity was obtained when compared to the bare PSF membrane of 18.2.

For MMMs with SSMMP/Im(nBu)Tf_2N, CO_2 permeability is not reduced as pure SSMMP, while N_2 permeability is kept practically constant compared to pure SSMMP (except at 3 wt%), increasing CO_2 selectivity to 71.9. The imidazolium-based ionic liquid containing Tf_2N as anion is widely known in literature for showing a strong affinity with CO_2. The CO_2 high solubility and selectivity in the presence of this IL are probably due to the presence of fluor and the size of the anion [80–83]. The sample with 3 wt% of filler presented a lower CO_2 selectivity and an increased permeability probably due to the filler agglomeration as depicted in SEM images.

For MMMs with SSMMP/Im(nBu)I, for all filler content, increased gas permeability was observed compared to bare PSF membrane. As previously seen in SEM images, filler agglomeration was observed even for low filler content, increasing gas permeation probably by forming preferential paths and decreasing CO_2 selectivity. Iodine anion and PSF membrane are incompatible, resulting in phase separation and defects formation, decreasing CO_2 selectivity.

Figure S8 summarizes the selectivity results for MMMs. When using SSMMP as filler, selectivity was superior for all filler content compared to bare PSF membrane, showing a good compatibility filler/matrix. The OH present in the SSMMP is probably responsible for this compatibility.

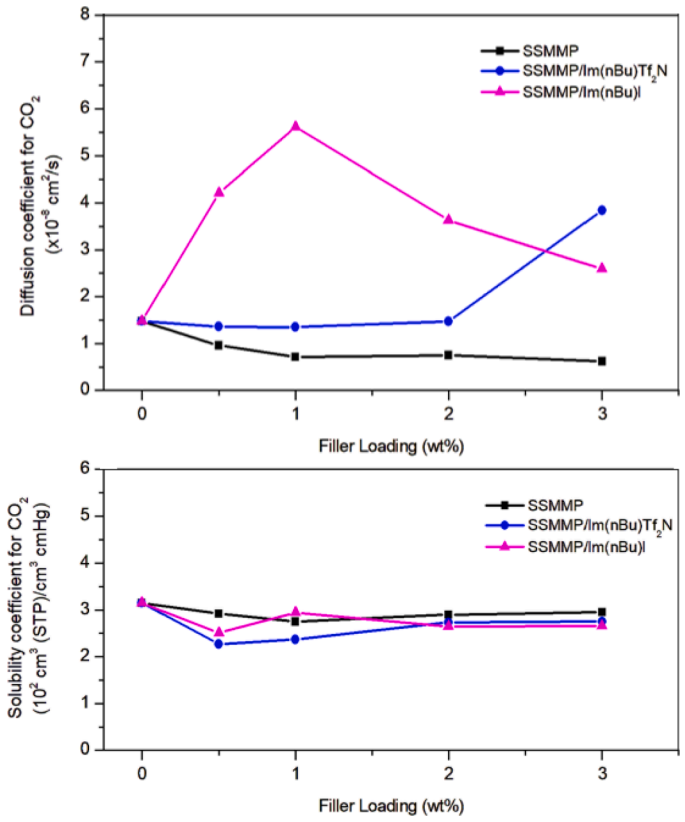

Fig. 8. Diffusion and solubility coefficients of SSMMP and SSMMP/ILs MMMs at 4 bar and 25 °C.

Similar result was obtained for SSMMP/Im(nBu)Tf_2N showing that the Tf_2N is a good filler/matrix compatibilizer besides having a good affinity for CO_2 corroborated by the high selectivity values when compared to bare PSF membranes and PSF-SSMMP MMM (see Table 4 and Figure S7). The iodine anion showed incompatibility with PSF resulting in membranes with low CO_2/N_2 selectivity (see Table 4 and Figure S8).

To gain further insight into the gas transport mechanism through the membranes, the diffusion and solubility coefficients for CO_2 were

Table 6
Comparing MMMs from literature and the present work.

Membrane	Filler/ Loading (wt %)	Pressure (bar)	Permeability CO_2 (barrer)	Selectivity CO_2/N_2	Ref
PSF	P–C15A / 1wt%	4	18.01	18.34	[71]
PSF	MCM-48 / 20wt%	4	18.21	23.65	[86]
PSF	GO / -	5	–	44.40	[74]
PSF	Pyrazole modified SBA-16 / 30wt%	10	14.43	46.13	[52]
PEBAX	[bmim] [Tf_2N]-ZIF-8 / 15wt%	1	104.90	83.9	[85]
PSF	RHS-AMP / 40wt%	10	8.46	33.31	[55]
PSF	SSMMP/ 0.5wt%	4	2.82	59.3	This work
PSF	SSMMP/Im (nBu)Tf_2N / 2wt%	4	4.03	71.9	This work
PSF	SSMMP/Im (nBu)I / 2wt %	4	9.62	24.3	This work

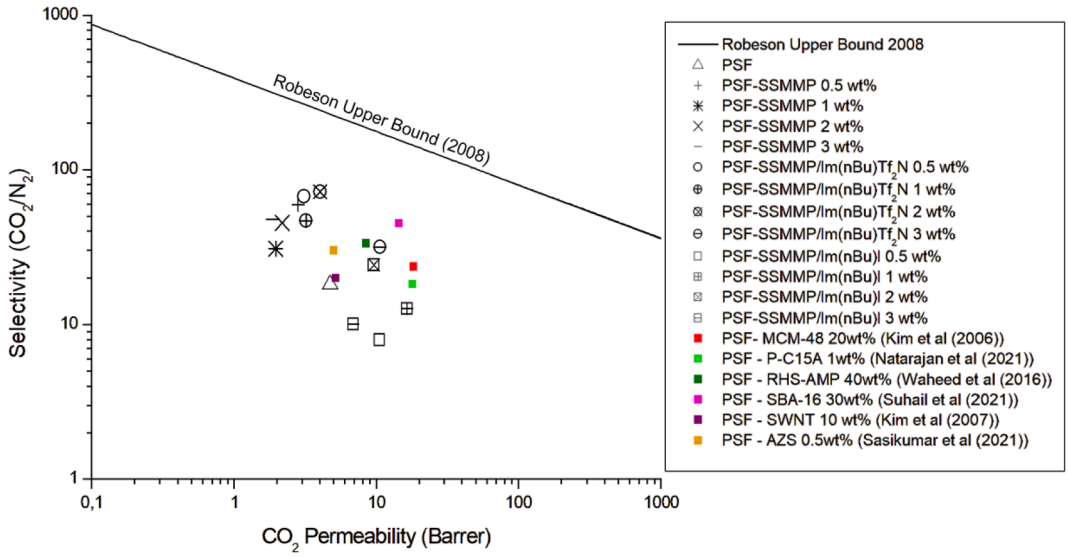

Fig. 9. MMMs and Robeson upper bound.

determined. These coefficients can provide a better understanding of the variations in permeability observed among different MMMs, as presented in Table 5 and Fig. 8.

The results for permeability and diffusivity were consistent, with diffusivity being the main contributor to the observed permeability in the samples. When there was an increase in permeability, the diffusivity of the sample to CO_2 also increased, while a decrease in permeability was accompanied by a decrease in CO_2 diffusivity. Addition of pure SSMMP resulted in reduced CO_2 diffusion coefficient, whereas incorporation of SSMMP with ionic liquid led to a gradual increase in CO_2 diffusion coefficient. This may be attributed to the presence of the ionic liquid, which can enhance diffusion. A similar finding was reported by Hudiono et al. [84] who observed an increase in permeability by increasing the charge of ionic liquids in SAPO-34, which resulted from greater gas diffusivity through the polymeric matrix.

The solubility coefficient, in turn, was less dominant in the transport mechanism, since the differences found between the samples are within the experimental error. Apparently, the slight decrease in solubility was compensated by the increase in CO_2 diffusivity.

The diffusion coefficients for nitrogen were not reported for the membranes, as estimation by the time-lag method introduces significant errors and biases in this case. These errors are likely due to the low permeability of the samples for N_2, as the diffusion process occurs very slowly, making it difficult to accurately measure and estimate the diffusion coefficients.

Table 6 presents a comparison regarding MMMs CO_2/N_2 selectivity and permeability results obtained in this work and the literature. The selectivity results when using SSMMP and SSMMP/ Im(nBu)Tf_2N are superior compared to the majority of MMMs described in literature, being inferior only to the MMMs using 15 wt% of ZIF-8 as filler (see Table 6) [85]. ZIF-8 is more expensive, with a more complicated synthesis when compared to pristine and IL-functionalized SSMMP, which are low-cost and energy-demand fillers.

Fig. 9 presents the Robeson Upper Bound [7] for CO_2/N_2 separation with bare PSF membrane, PSF-SSMMP and PSF-SSMMP/IL MMMs. The use of SSMMP and SSMMP/IL as fillers considerably increases the separation properties of PSF. Despite the good selectivity, the low permeability needs still to be improved to surpass the Robeson Upper Bound.

MMMs using SSMMP and SSMMP/Im(nBu)Tf_2N as fillers can be used for CO_2 separation from post-combustion gasses presenting a high selectivity. Membranes with SSMMP/Im(nBu)I had an increase in permeability to CO_2, with a drastic reduction in selectivity. Based on the simulation study presented in literature [87], the combination of the two membranes can offer a good alternative for CO_2 separation: one membrane with high selectivity combined with a membrane with high permeability. Yet, future studies may focus on using a polymer matrix with greater CO_2 permeability than polysulfone, such as PEBAX, Matrimid, among others, and then verify the change in permeability and selectivity parameters in the Robeson Upper Bound.

4. Conclusion

As far as we know here, we reported for the first time the use of SSMMP and SSMMP/IL as filler in mixed matrix membranes. Polysulfone-based membranes were successfully produced, leading to a uniform filler distribution in an adequate filler concentration. The presence of hydroxyl groups in the fillers strengthened polymer/filler interaction. Compared to pristine SSMMP, SSMMP/Im(nBu)Tf_2N showed superior interfacial compatibility with PSF, leading to a uniform charge distribution in the polymer matrix. SSMMP/Im(nBu)I showed poor compatibility with PSF, corroborated by the presence of particles agglomerates. The addition of SSMMP to the membrane increases the selectivity for the CO_2/N_2 mixture, whereas SSMMP/Im(nBu)Tf_2N increases both permeability and selectivity, indicating better affinity with CO_2. The membranes have high separation performance, with the best result obtained with PSF-SSMMP/Im(nBu)Tf_2N 2 wt% sample with a CO_2/N_2 selectivity of 71.9, an increase of 295% compared to bare PSF. These results evidenced that the use of SSMMP and SSMMP/IL are promising for use in post-combustion process due to low-cost reagents needed for theis synthesis, low energy consumption and easy synthesis, besides no heating steps nor need for calcination unlike other materials presented in literature as suitable fillers for MMMs.

Funding

This study was written by some members of the Capes- PRINT Internationalization Project from PUCRS University and was financed in part by the Coordination for the Improvement of Higher Education Personnel- Brasil (CAPES) – Finance Code 001. Henrique Ferrari and Daniela M. Rodrigues thank CAPES; Sandra Einloft thanks CNPq for research scholarship. This study was financed in part by the Coordenação de Aperfeiçoamento de Pessoal de Nível Superior – Brasil (CAPES) – Finance Code 001.

Declaration of Competing Interest

The authors declare that they have no known competing financial interests or personal relationships that could have appeared to influence the work reported in this paper.

Data availability

No data was used for the research described in the article.

Acknowledgments

This study was written by some members of the Capes- PRINT Internationalization Project from PUCRS University and was financed in part by the Coordination for the Improvement of Higher Education Personnel- Brasil (CAPES) – Finance Code 001. Henrique Ferrari and Daniela M. Rodrigues thank CAPES; Sandra Einloft thanks CNPq for research scholarship. This study was financed in part by the Coordenação de Aperfeiçoamento de Pessoal de Nível Superior – Brasil (CAPES) – Finance Code 001.

Supplementary materials

Supplementary material associated with this article can be found, in the online version, at doi:10.1016/j.ceja.2023.100488.

References

[1] R. Chang, X. Wu, O. Cheung, W. Liu, Synthetic solid oxide sorbents for CO 2 capture: state-of-the art and future perspectives, (2022). https://doi.org/10.1039/d1ta07697c.
[2] M. Kárászová, B. Zach, Z. Petrusová, V. Červenka, M. Bobák, M. Šyc, P. Izák, Post-combustion carbon capture by membrane separation, Rev., Sep. Purif. Technol. 238 (2020), 116448, https://doi.org/10.1016/J.SEPPUR.2019.116448.
[3] A. Brunetti, F. Scura, G. Barbieri, E. Drioli, Membrane technologies for CO2 separation, J. Memb. Sci. 359 (2010) 115–125, https://doi.org/10.1016/J.MEMSCI.2009.11.040.
[4] L. Zhao, E. Riensche, R. Menzer, L. Blum, D. Stolten, A parametric study of CO2/N2 gas separation membrane processes for post-combustion capture, J. Memb. Sci. 325 (2008) 284–294, https://doi.org/10.1016/J.MEMSCI.2008.07.058.
[5] A.R. Kamble, C.M. Patel, Z.V.P. Murthy, A review on the recent advances in mixed matrix membranes for gas separation processes, Renew. Sustain. Energy Rev. 145 (2021), 111062, https://doi.org/10.1016/J.RSER.2021.111062.
[6] Y. Han, W.S.W. Ho, Polymeric membranes for CO2 separation and capture, J. Memb. Sci. 628 (2021), 119244, https://doi.org/10.1016/J.MEMSCI.2021.119244.
[7] L.M. Robeson, The upper bound revisited, J. Memb. Sci. 320 (2008) 390–400, https://doi.org/10.1016/J.MEMSCI.2008.04.030.
[8] S.H. Goh, H.S. Lau, W.F. Yong, Metal–organic frameworks (MOFs)-based mixed matrix membranes (MMMs) for gas separation: a review on advanced materials in harsh environmental applications, Small 18 (2022), https://doi.org/10.1002/smll.202107536.
[9] Ş.B. Tantekin-Ersolmaz, Ç. Atalay-Oral, M. Tatlier, A. Erdem-Şenatalar, B. Schoeman, J. Sterte, Effect of zeolite particle size on the performance of polymer–zeolite mixed matrix membranes, J. Memb. Sci. 175 (2000) 285–288, https://doi.org/10.1016/S0376-7388(00)00423-3.
[10] B. Zornoza, S. Irusta, C.T. Ellez, J.In Coronas, Mesoporous silica sphere-polysulfone mixed matrix membranes for gas separation, (2009). https://doi.org/10.1021/la900656z.
[11] W. Guan, Y. Dai, C. Dong, X. Yang, Y. Xi, Zeolite imidazolate framework (ZIF)-based mixed matrix membranes for CO 2 separation: a review, (2020). https://doi.org/10.1002/app.48968.
[12] M.M. Zagho, M.K. Hassan, M. Khraisheh, M.A.A. Al-Maadeed, S. Nazarenko, A review on recent advances in CO2 separation using zeolite and zeolite-like materials as adsorbents and fillers in mixed matrix membranes (MMMs), Chem. Eng. J. Adv. 6 (2021), 100091, https://doi.org/10.1016/J.CEJA.2021.100091.
[13] W.K. Setiawan, K.Y. Chiang, Silica applied as mixed matrix membrane inorganic filler for gas separation: a review, Sustain. Environ. Res. 1 (2019), https://doi.org/10.1186/s42834-019-0028-1.
[14] E. Nezhadmoghadam, P. Chenar, M. Omidkhah, A. Nezhadmoghadam, R. Abedini, Aminosilane grafted Matrimid 5218/nano-silica mixed matrix membrane for CO 2 /light gases separation, Korean J. Chem. Eng. 35 (2018) 526–534, https://doi.org/10.1007/s11814-017-0282-z.
[15] S. Hassanajili, E. Masoudi, G. Karimi, M. Khademi, Mixed matrix membranes based on polyetherurethane and polyesterurethane containing silica nanoparticles for separation of CO2/CH4 gases, Sep. Purif. Technol. 116 (2013) 1–12, https://doi.org/10.1016/J.SEPPUR.2013.05.017.
[16] M. Waqas Anjum, F. de Clippel, J. Didden, A. Laeeq Khan, S. Couck, G.V. Baron, J. F.M. Denayer, B.F. Sels, I.F.J. Vankelecom, Polyimide mixed matrix membranes for CO2 separations using carbon–silica nanocomposite fillers, J. Memb. Sci. 495 (2015) 121–129, https://doi.org/10.1016/J.MEMSCI.2015.08.006.
[17] R. Borgohain, N. Jain, B. Prasad, B. Mandal, B. Su, Carboxymethyl chitosan/carbon nanotubes mixed matrix membranes for CO2 separation, React. Funct. Polym. 143 (2019), 104331, https://doi.org/10.1016/J.REACTFUNCTPOLYM.2019.104331.
[18] D. Wang, D. Yao, Y. Wang, F. Wang, Y. Xin, S. Song, Z. Zhang, F. Su, Y. Zheng, Carbon nanotubes and graphene oxide-based solvent-free hybrid nanofluids functionalized mixed-matrix membranes for efficient CO2/N2 separation, Sep. Purif. Technol. 221 (2019) 421–432, https://doi.org/10.1016/J.SEPPUR.2019.04.005.
[19] A.M. Norouzi, M. Elyasi Kojabad, M. Chapalaghi, A. Hosseinkhani, A. Arabloo nareh, E. Nemati Lay, Polyester-based polyurethane mixed-matrix membranes incorporating carbon nanotube-titanium oxide coupled nanohybrid for carbon dioxide capture enhancement: molecular simulation and experimental study, J. Mol. Liq. 360 (2022), 119540, https://doi.org/10.1016/J.MOLLIQ.2022.119540.
[20] S. Basu, A. Cano-Odena, I.F.J. Vankelecom, MOF-containing mixed-matrix membranes for CO2/CH4 and CO2/N2 binary gas mixture separations, Sep. Purif. Technol. 81 (2011) 31–40, https://doi.org/10.1016/J.SEPPUR.2011.06.037.
[21] M.Z. Ahmad, T.A. Peters, N.M. Konnertz, T. Visser, C. Téllez, J. Coronas, V. Fila, W. M. de Vos, N.E. Benes, High-pressure CO2/CH4 separation of Zr-MOFs based mixed matrix membranes, Sep. Purif. Technol. 230 (2020), 115858, https://doi.org/10.1016/J.SEPPUR.2019.115858.
[22] W. Chen, Z. Zhang, C. Yang, J. Liu, H. Shen, K. Yang, Z. Wang, PIM-based mixed-matrix membranes containing MOF-801/ionic liquid nanocomposites for enhanced CO2 separation performance, J. Memb. Sci. 636 (2021), 119581, https://doi.org/10.1016/J.MEMSCI.2021.119581.
[23] I.C. Ferreira, T.J. Ferreira, A.D.S. Barbosa, B. de Castro, R.P.P.L. Ribeiro, J.P. B. Mota, V.D. Alves, L. Cunha-Silva, I.A.A.C. Esteves, L.A. Neves, Cr-based MOF/IL composites as fillers in mixed matrix membranes for CO2 separation, Sep. Purif. Technol. 276 (2021), 119303, https://doi.org/10.1016/J.SEPPUR.2021.119303.
[24] S.N. Wijenayake, N.P. Panapitiya, S.H. Versteeg, C.N. Nguyen, S. Goel, K.J. Balkus, I.H. Musselman, J.P. Ferraris, Surface cross-linking of ZIF-8/polyimide mixed matrix membranes (MMMs) for gas separation, Ind. Eng. Chem. Res. 52 (2013) 6991–7001, https://doi.org/10.1021/ie400149e.
[25] J. Shen, M. Zhang, G. Liu, K. Guan, W. Jin, Size effects of graphene oxide on mixed matrix membranes for CO2 separation, AIChE J 62 (2016) 2843–2852, https://doi.org/10.1002/aic.15260.
[26] J. Zhang, Q. Xin, X. Li, M. Yun, R. Xu, S. Wang, Y. Li, L. Lin, X. Ding, H. Ye, Y. Zhang, Mixed matrix membranes comprising aminosilane-functionalized graphene oxide for enhanced CO2 separation, J. Memb. Sci. 570–571 (2019) 343–354, https://doi.org/10.1016/J.MEMSCI.2018.10.075.
[27] M. Vinoba, M. Bhagiyalakshmi, Y. Alqaheem, A.A. Alomair, A. Pérez, M.S. Rana, Recent progress of fillers in mixed matrix membranes for CO2 separation: a review, Sep. Purif. Technol. 188 (2017) 431–450, https://doi.org/10.1016/J.SEPPUR.2017.07.051.
[28] H. Wu, X. Li, Y. Li, S. Wang, R. Guo, Z. Jiang, C. Wu, Q. Xin, X. Lu, Facilitated transport mixed matrix membranes incorporated with amine functionalized MCM-41 for enhanced gas separation properties, J. Memb. Sci. 465 (2014) 78–90, https://doi.org/10.1016/J.MEMSCI.2014.04.023.
[29] K. Kalantari, P. Moradihamedani, N.A. Ibrahim, A.H. Bin Abdullah, A.B.M. Afifi, Polysulfone mixed-matrix membrane incorporating talc clay particles for gas separation, Polym. Bull. 75 (2018) 3723–3738, https://doi.org/10.1007/s00289-017-2234-5.
[30] M. Blanchard, M. Méheut, L. Delon, M. Poirier, P. Micoud, C.Le Roux, F. Martin, Infrared spectroscopic study of the synthetic Mg–Ni talc series, Phys. Chem. Miner. 45 (2018) 843–854, https://doi.org/10.1007/s00269-018-0966-x.
[31] A. Dumas, F. Martin, E. Ferrage, P. Micoud, C.Le Roux, S. Petit, Synthetic talc advances: coming closer to nature, added value, and industrial requirements, Appl. Clay Sci. 85 (2013) 8–18, https://doi.org/10.1016/J.CLAY.2013.09.006.
[32] A. Dumas, M. Mizrahi, F. Martin, F.G. Requejo, Local and extended-order evolution of synthetic talc during hydrothermal synthesis: extended x-ray absorption fine structure, x-ray diffraction, and Fourier transform infrared spectroscopy studies, Cryst. Growth Des. 15 (2015) 5451–5463, https://doi.org/10.1021/acs.cgd.5b01076.
[33] A. Dumas, F. Martin, C.Le Roux, P. Micoud, S. Petit, E. Ferrage, J. Brendlé, O. Grauby, M. Greenhill-Hooper, Phyllosilicates synthesis: a way of accessing edges contributions in NMR and FTIR spectroscopies. Example of synthetic talc, Phys. Chem. Miner. 40 (2013) 361–373, https://doi.org/10.1007/s00269-013-0577-5.
[34] M. Claverie, A. Dumas, C. Carême, M. Poirier, C.Le Roux, P. Micoud, F. Martin, C. Aymonier, Synthetic talc and talc-like structures: preparation, features and applications, Chem. - A Eur. J 24 (2018) 519–542, https://doi.org/10.1002/chem.201702763.
[35] G. Dias, M. Prado, C.Le Roux, M. Poirier, P. Micoud, R. Ligabue, F. Martin, S. Einloft, Synthetic talc as catalyst and filler for waterborne polyurethane-based nanocomposite synthesis, Polym. Bull. 77 (2020) 975–987, https://doi.org/10.1007/s00289-019-02789-w.
[36] L.M. dos Santos, R. Ligabue, A. Dumas, C. Le Roux, P. Micoud, J.F. Meunier, F. Martin, M. Corvo, P. Almeida, S. Einloft, Waterborne polyurethane/Fe3O4-synthetic talc composites: synthesis, characterization, and magnetic properties, Polym. Bull. 75 (2018) 1915–1930, https://doi.org/10.1007/s00289-017-2133-9.

[37] M. Yousfi, S. Livi, A. Dumas, C.Le Roux, J. Crépin-Leblond, M. Greenhill-Hooper, J. Duchet-Rumeau, Use of new synthetic talc as reinforcing nanofillers for polypropylene and polyamide 6 systems: thermal and mechanical properties, J. Colloid Interface Sci. 403 (2013) 29–42, https://doi.org/10.1016/J.JCIS.2013.04.019.
[38] D. Rodrigues, F. Bernard, C.Le Roux, E. Duarte, P. Micoud, A. Castillo, F. Martin, S. Einloft, Synthetic silico-metallic mineral particles SSMMP: a new option for CO2 capture and CO2/N2 separation from post-combustion technology, Appl. Clay Sci. 226 (2022), 106572, https://doi.org/10.1016/J.CLAY.2022.106572.
[39] A. Kaithwas, M. Prasad, A. Kulshreshtha, S. Verma, Industrial wastes derived solid adsorbents for CO2 capture: a mini review, Chem. Eng. Res. Des. 90 (2012) 1632–1641, https://doi.org/10.1016/J.CHERD.2012.02.011.
[40] A. Dindi, D.V. Quang, L.F. Vega, E. Nashef, M.R.M. Abu-Zahra, Applications of fly ash for CO2 capture, utilization, and storage, J. CO2 Util. 29 (2019) 82–102, https://doi.org/10.1016/J.JCOU.2018.11.011.
[41] H.T. Jang, Y.K. Park, Y.S. Ko, J.Y. Lee, B. Margandan, Highly siliceous MCM-48 from rice husk ash for CO2 adsorption, Int. J. Greenh. Gas Control. 3 (2009) 545–549, https://doi.org/10.1016/J.IJGGC.2009.02.008.
[42] M.M. Wan, H.Y. Zhu, Y.Y. Li, J. Ma, S. Liu, J.H. Zhu, Novel CO2-capture derived from the basic ionic liquids orientated on mesoporous materials, ACS Appl. Mater. Interfaces 6 (2014) 12947–12955, https://doi.org/10.1021/am5028814.
[43] M. Hasib-ur-Rahman, M. Siaj, F. Larachi, Ionic liquids for CO2 capture—development and progress, Chem. Eng. Process. Process Intensif. 49 (2010) 313–322, https://doi.org/10.1016/J.CEP.2010.03.008.
[44] M. Mohamedali, H. Ibrahim, A. Henni, Imidazolium based ionic liquids confined into mesoporous silica MCM-41 and SBA-15 for carbon dioxide capture, Microporous Mesoporous Mater. 294 (2020), 109916, https://doi.org/10.1016/J.MICROMESO.2019.109916.
[45] G. Huang, A.P. Isfahani, A. Muchtar, K. Sakurai, B.B. Shrestha, D. Qin, D. Yamaguchi, E. Sivaniah, B. Ghalei, Pebax/ionic liquid modified graphene oxide mixed matrix membranes for enhanced CO2 capture, J. Memb. Sci. 565 (2018) 370–379, https://doi.org/10.1016/J.MEMSCI.2018.08.026.
[46] O.S. Serbanescu, S.I. Voicu, V.K. Thakur, Polysulfone functionalized membranes: properties and challenges, Mater. Today Chem. 17 (2020), 100302, https://doi.org/10.1016/J.MTCHEM.2020.100302.
[47] M. Farrokhara, F. Dorosti, New high permeable polysulfone/ionic liquid membrane for gas separation, Chinese J. Chem. Eng. 28 (2020) 2301–2311, https://doi.org/10.1016/j.cjche.2020.04.002.
[48] S. Kim, L. Chen, J.K. Johnson, E. Marand, Polysulfone and functionalized carbon nanotube mixed matrix membranes for gas separation: theory and experiment, J. Memb. Sci. 294 (2007) 147–158, https://doi.org/10.1016/J.MEMSCI.2007.02.028.
[49] P.V. Chai, E. Mahmoudi, Y.H. Teow, A.W. Mohammad, Preparation of novel polysulfone-Fe3O4/GO mixed-matrix membrane for humic acid rejection, J. Water Process Eng. 15 (2017) 83–88, https://doi.org/10.1016/J.JWPE.2016.06.001.
[50] J. Ahn, W.J. Chung, I. Pinnau, M.D. Guiver, Polysulfone/silica nanoparticle mixed-matrix membranes for gas separation, J. Memb. Sci. 314 (2008) 123–133, https://doi.org/10.1016/J.MEMSCI.2008.01.031.
[51] I.U. Khan, M.H.D. Othman, A. Jilani, A.F. Ismail, H. Hashim, J. Jaafar, A. K. Zulhairun, M.A. Rahman, G.U. Rehman, ZIF-8 based polysulfone hollow fiber membranes for natural gas purification, Polym. Test. 84 (2020), 106415, https://doi.org/10.1016/J.POLYMERTESTING.2020.106415.
[52] F. Suhail, M. Batool, A.T. Shah, S. Tabassum, A.L. Khan, M.A. Gilani, Highly CO2 selective mixed matrix membranes of polysulfone based on hetaryl modified SBA-16 particles, Sep. Purif. Technol. 258 (2021), 117999, https://doi.org/10.1016/J.SEPPUR.2020.117999.
[53] M. Laghaei, M. Sadeghi, B. Ghalei, M. Shahrooz, The role of compatibility between polymeric matrix and silane coupling agents on the performance of mixed matrix membranes: polyethersulfone/MCM-41, J. Memb. Sci. 513 (2016) 20–32, https://doi.org/10.1016/J.MEMSCI.2016.04.039.
[54] F. Dorosti, M.R. Omidkhah, M.Z. Pedram, F. Moghadam, Fabrication and characterization of polysulfone/polyimide-zeolite mixed matrix membrane for gas separation, Chem. Eng. J. 171 (2011) 1469–1476, https://doi.org/10.1016/j.cej.2011.05.081.
[55] N. Waheed, A. Mushtaq, S. Tabassum, M.A. Gilani, A. Ilyas, F. Ashraf, Y. Jamal, M. R. Bilad, A.U. Khan, A.L. Khan, Mixed matrix membranes based on polysulfone and rice husk extracted silica for CO2 separation, Sep. Purif. Technol. 170 (2016) 122–129, https://doi.org/10.1016/j.seppur.2016.06.035.
[56] H. Wu, J. Thibault, B. Kruczek, The validity of the time-lag method for the characterization of mixed-matrix membranes, J. Memb. Sci. 618 (2021), 118715, https://doi.org/10.1016/j.memsci.2020.118715.
[57] B.B. Polesso, F.L. Bernard, H.Z. Ferrari, E.A. Duarte, F.D. Vecchia, S. Einloft, Supported ionic liquids as highly efficient and low-cost material for CO2/CH4 separation process, Heliyon 5 (2019) e02183, https://doi.org/10.1016/J.HELIYON.2019.E02183.
[58] Z. Shi, Q. Su, T. Ying, X. Tan, L. Deng, L. Dong, W. Cheng, Ionic liquids with multiple active sites supported by SBA-15 for catalyzing conversion of CO2 into cyclic carbonates, J. CO2 Util. 39 (2020), 101162, https://doi.org/10.1016/J.JCOU.2020.101162.
[59] J. Zhao, H. Xu, D. Tang, J.P. Mathews, S. Li, S. Tao, A comparative evaluation of coal specific surface area by CO2 and N2 adsorption and its influence on CH4 adsorption capacity at different pore sizes, Fuel 183 (2016) 420–431, https://doi.org/10.1016/J.FUEL.2016.06.076.
[60] N.C.S. Selvam, R.T. Kumar, L.J. Kennedy, J.J. Vijaya, Comparative study of microwave and conventional methods for the preparation and optical properties of novel MgO-micro and nano-structures, J. Alloys Compd. 509 (2011) 9809–9815, https://doi.org/10.1016/J.JALLCOM.2011.08.032.
[61] A. Ansari, A. Ali, M. Asif, Shamsuzzaman, Microwave-assisted MgO NP catalyzed one-pot multicomponent synthesis of polysubstituted steroidal pyridines, New J. Chem. 42 (2018) 184–197, https://doi.org/10.1039/c7nj03742b.
[62] H. Molavi, A. Eskandari, A. Shojaei, S.A. Mousavi, Enhancing CO2/N2 adsorption selectivity via post-synthetic modification of NH2-UiO-66(Zr), Microporous Mesoporous Mater 257 (2018) 193–201, https://doi.org/10.1016/J.MICROMESO.2017.08.043.
[63] H. Yang, C. Du, Y. Hu, S. Jin, W. Yang, A. Tang, E.G. Avvakumov, Preparation of porous material from talc by mechanochemical treatment and subsequent leaching, Appl. Clay Sci. 31 (2006) 290–297, https://doi.org/10.1016/j.clay.2005.10.015.
[64] K.S. Kim, K.H. Lee, K. Cho, C.E. Park, Surface modification of polysulfone ultrafiltration membrane by oxygen plasma treatment, J. Memb. Sci. 199 (2002) 135–145, https://doi.org/10.1016/S0376-7388(01)00686-X.
[65] H. Fan, C. Wang, Y. Li, Y. Wei, Preparation and anti-protein fouling property of δ-gluconolactone-modified hydrophilic polysulfone membranes, J. Memb. Sci. 415–416 (2012) 161–167, https://doi.org/10.1016/j.memsci.2012.04.047.
[66] N. Sieffert, G. Wipff, The [BMI][Tf2N] ionic liquid/water binary system: a molecular dynamics study of phase separation and of the liquid-liquid interface, J. Phys. Chem. B. 110 (2006) 13076–13085, https://doi.org/10.1021/jp061849q.
[67] T. Erdmenger, J. Vitz, F. Wiesbrock, U.S. Schubert, Influence of different branched alkyl side chains on the properties of imidazolium-based ionic liquids, J. Mater. Chem. 18 (2008) 5267–5273, https://doi.org/10.1039/b807119e.
[68] J.G. Huddleston, A.E. Visser, W.M. Reichert, H.D. Willauer, G.A. Broker, R. D. Rogers, Characterization and comparison of hydrophilic and hydrophobic room temperature ionic liquids incorporating the imidazolium cation, Green Chem 3 (2001) 156–164, https://doi.org/10.1039/b103275p.
[69] M. Wang, Z. Wang, S. Zhao, J. Wang, S. Wang, Recent advances on mixed matrix membranes for CO2 separation, Chinese J. Chem. Eng. 25 (2017) 1581–1597, https://doi.org/10.1016/J.CJCHE.2017.07.006.
[70] B. Sasikumar, G. Arthanareeswaran, K. Sankaranarayanan, K. Jeyadheepan, Synthesis and formation of phase-tuned TiO2-/ionic liquid-incorporated polymeric membranes for ammonia sensing at room temperature, ACS Sustain. Chem. Eng. (2019), https://doi.org/10.1021/acssuschemeng.9b01850.
[71] P. Natarajan, B. Sasikumar, S. Elakkiya, G. Arthanareeswaran, A.F. Ismail, W. Youravong, E. Yuliwati, Pillared cloisite 15A as an enhancement filler in polysulfone mixed matrix membranes for CO2/N2 and O2/N2 gas separation, J. Nat. Gas Sci. Eng. 86 (2021), 103720, https://doi.org/10.1016/J.JNGSE.2020.103720.
[72] M. Nisar, F.L. Bernard, E. Duarte, V.V. Chaban, S. Einloft, New polysulfone microcapsules containing metal oxides and ([BMIM][NTf2]) ionic liquid for CO2capture, J. Environ. Chem. Eng. 9 (2021), https://doi.org/10.1016/j.jece.2020.104781.
[73] S. Rafiq, Z. Man, A. Maulud, N. Muhammad, S. Maitra, Separation of CO2 from CH4 using polysulfone/polyimide silica nanocomposite membranes, Sep. Purif. Technol. 90 (2012) 162–172, https://doi.org/10.1016/J.SEPPUR.2012.02.031.
[74] K. Zahri, K.C. Wong, P.S. Goh, A.F. Ismail, Graphene oxide/polysulfone hollow fiber mixed matrix membranes for gas separation, RSC Adv 6 (2016) 89130–89139, https://doi.org/10.1039/c6ra16820e.
[75] S. Shahid, K. Nijmeijer, S. Nehache, I. Vankelecom, A. Deratani, D. Quemener, MOF-mixed matrix membranes: precise dispersion of MOF particles with better compatibility via a particle fusion approach for enhanced gas separation properties, J. Memb. Sci. 492 (2015) 21–31, https://doi.org/10.1016/J.MEMSCI.2015.05.015.
[76] E. Ghasemi Estahbanati, M. Omidkhah, A. Ebadi Amooghin, Preparation and characterization of novel Ionic liquid/Pebax membranes for efficient CO2/light gases separation, J. Ind. Eng. Chem. 51 (2017) 77–89, https://doi.org/10.1016/J.JIEC.2017.02.017.
[77] S.K. Chaurasia, R.K. Singh, S. Chandra, Thermal Stability, Complexing behavior, and ionic transport of polymeric gel membranes based on polymer PVdF-HFP and ionic liquid, [BMIM][BF 4], (2012). https://doi.org/10.1021/jp307694q.
[78] R. Rezaee, S. Nasseri, A.H. Mahvi, R. Nabizadeh, S.A. Mousavi, A. Rashidi, A. Jafari, S. Nazmara, Fabrication and characterization of a polysulfone-graphene oxide nanocomposite membrane for arsenate rejection from water, J. Environ. Heal. Sci. Eng. 13 (2015), https://doi.org/10.1186/s40201-015-0217-8.
[79] S. Zinadini, A.A. Zinatizadeh, M. Rahimi, V. Vatanpour, H. Zangeneh, Preparation of a novel antifouling mixed matrix PES membrane by embedding graphene oxide nanoplates, J. Memb. Sci. 453 (2014) 292–301, https://doi.org/10.1016/j.memsci.2013.10.070.
[80] O. Yuksel Orhan, Effects of various anions and cations in ionic liquids on CO2 capture, J. Mol. Liq. 333 (2021), 115981, https://doi.org/10.1016/J.MOLLIQ.2021.115981.
[81] A.S. Aquino, F.L. Bernard, J.V. Borges, L. Mafra, F. Dalla Vecchia, M.O. Vieira, R. Ligabue, M. Seferin, V.V. Chaban, E.J. Cabrita, S. Einloft, Rationalizing the role of the anion in CO 2 capture and conversion using imidazolium-based ionic liquid modified mesoporous silica †, (2015). https://doi.org/10.1039/c5ra07561k.
[82] X. Zhang, X. Zhang, H. Dong, Z. Zhao, S. Zhang, Y. Huang, Carbon capture with ionic liquids: overview and progress †. 10.1039/c2ee21152a.
[83] F.L. Bernard, E.A. Duarte, B.B. Polesso, R.B. Duczinski, S. Einloft, CO2 sorption using encapsulated imidazolium-based fluorinated ionic liquids, Environ. Challenges 4 (2021), 100109, https://doi.org/10.1016/J.ENVC.2021.100109.
[84] Y.C. Hudiono, T.K. Carlisle, A.L. LaFrate, D.L. Gin, R.D. Noble, Novel mixed matrix membranes based on polymerizable room-temperature ionic liquids and SAPO-34 particles to improve CO2 separation, J. Memb. Sci. 370 (2011) 141–148, https://doi.org/10.1016/j.memsci.2011.01.012.

[85] H. Li, L. Tuo, K. Yang, H.K. Jeong, Y. Dai, G. He, W. Zhao, Simultaneous enhancement of mechanical properties and CO2 selectivity of ZIF-8 mixed matrix membranes: interfacial toughening effect of ionic liquid, J. Memb. Sci. 511 (2016) 130–142, https://doi.org/10.1016/J.MEMSCI.2016.03.050.

[86] S. Kim, E. Marand, J. Ida, V.V. Guliants, Polysulfone and mesoporous molecular sieve MCM-48 mixed matrix membranes for gas separation, Chem. Mater. 18 (2006) 1149–1155, https://doi.org/10.1021/cm052305o.

[87] L. Giordano, D. Roizard, E. Favre, Life cycle assessment of post-combustion CO2 capture: a comparison between membrane separation and chemical absorption processes, Int. J. Greenh. Gas Control. 68 (2018) 146–163, https://doi.org/10.1016/J.IJGGC.2017.11.008.